






Article

Lactones from the Sponge-Derived Fungus *Talaromyces rugulosus*

Lisa Küppers^{1,†}, Weaam Ebrahim^{1,2,†} , Mona El-Neketi², Ferhat C. Özkaya¹ ,
Attila Mándi³ , Tibor Kurtán³, Raha S. Orfali⁴, Werner E. G. Müller⁵, Rudolf Hartmann⁶ ,
Wenhan Lin⁷, Weiguo Song⁸, Zhen Liu^{1,*}  and Peter Proksch^{1,*}

¹ Institute of Pharmaceutical Biology and Biotechnology, Heinrich-Heine-Universität Düsseldorf, 40225 Düsseldorf, Germany; li-kue@gmx.de (L.K.); weaam.ebrahim@uni-duesseldorf.de (W.E.); fcanozkaya@gmail.com (F.C.Ö.)

² Department of Pharmacognosy, Faculty of Pharmacy, Mansoura University, Mansoura 35516, Egypt; monaneketi@yahoo.com

³ Department of Organic Chemistry, University of Debrecen, 4032 Debrecen, Hungary; mandi.attila@science.unideb.hu (A.M.); kurtan.tibor@science.unideb.hu (T.K.)

⁴ Department of Pharmacognosy, Faculty of Pharmacy, King Saud University, Riyadh 11451, Saudi Arabia; rom2leen@gmail.com

⁵ Institute of Physiological Chemistry, Universitätsmedizin der Johannes Gutenberg-Universität Mainz, 55128 Mainz, Germany; wmueller@uni-mainz.de

⁶ Institute of Complex Systems: Strukturbiochemie, Forschungszentrum Juelich, 52428 Juelich, Germany; r.hartmann@fz-juelich.de

⁷ State Key Laboratory of Natural and Biomimetic Drugs, Peking University, Beijing 100191, China; whlin@bjmu.edu.cn

⁸ FukangPharma, North-East of Dongwaihuan Road, Dongcheng Industrial Area, Shouguang City 262700, China; songwg@139.com

* Correspondence: zhenfeizi0@sina.com (Z.L.); proksch@uni-duesseldorf.de (P.P.); Tel.: +49-211-81-14163 (P.P.)

† These authors contributed equally to this work.

Received: 12 October 2017; Accepted: 9 November 2017; Published: 14 November 2017

Abstract: The marine-derived fungus *Talaromyces rugulosus* isolated from the Mediterranean sponge *Axinella cannabina* and cultured on solid rice medium yielded seventeen lactone derivatives including five butenolides (1–5), seven (3S)-resorcylic acid derivatives (6–12), two butenolide-resorcylic acid dimers (13 and 14), and three dihydroisocoumarins (15–17). Among them, fourteen compounds (1–3, 6–16) are new natural products. The structures of the isolated compounds were elucidated by 1D and 2D NMR (Nuclear Magnetic Resonance) spectroscopy as well as by ESI-HRMS (ElectroSpray Ionization-High Resolution Mass Spectrometry). TDDFT-ECD (Time-Dependent Density Functional Theory-Electronic Circular Dichroism) calculations were performed to determine the absolute configurations of chiral compounds. The butenolide-resorcylic acid dimers talarodilactones A and B (13 and 14) exhibited potent cytotoxicity against the L5178Y murine lymphoma cell line with IC₅₀ values of 3.9 and 1.3 μM, respectively.

Keywords: *Talaromyces rugulosus*; lactones; ECD calculation; cytotoxicity

1. Introduction

Marine-derived fungi are prolific sources for bioactive secondary metabolites, such as the famous antibiotic cephalosporin C obtained from the fungus *Acremonium chrysogenum* [1], or halimide derived from an algiculous fungus, which gave rise to the semisynthetic metabolite plinabulin that is now in Phase II clinical studies for its anticancer potential against either solid tumours or lymphomas [2,3].

During our ongoing search for new bioactive secondary metabolites from fungal origin [4–7], we investigated *Talaromyces rugulosus*, which was isolated from the Mediterranean sponge *Axinella cannabina*. The fungal genus *Talaromyces* is known to produce diverse bioactive secondary metabolites including tetraene lactones [8], polyketides [9,10], alkaloids and peptides with some of them exhibiting antibiotic, cytotoxic and anti-HBV (Hepatitis B Virus) activities [11]. Only a few research papers are devoted to the chemical constituents of *Talaromyces rugulosus*. Yilmaz et al. reported the isolation of skyrin, endocrocin, emodin, prugosins A–C and a bis-anthraquinoid pigment, rugulosin A, which showed antibacterial activity against *Staphylococcus aureus* [12]. This encouraged us to investigate the natural products of the sponge-derived strain of *T. rugulosus*.

The EtOAc (ethyl acetate) extract of the fungus when fermented on solid rice medium yielded three new butenolides (1–3), seven new resorcylic derivatives (6–12), two new butenolide-resorcylic dimers (13 and 14) and two new dihydroisocoumarins (15 and 16) as well as three known analogues (4, 5 and 17) (Figure 1). The structure elucidation including the absolute configuration assignment and biological activities of the isolated compounds are discussed in this report.

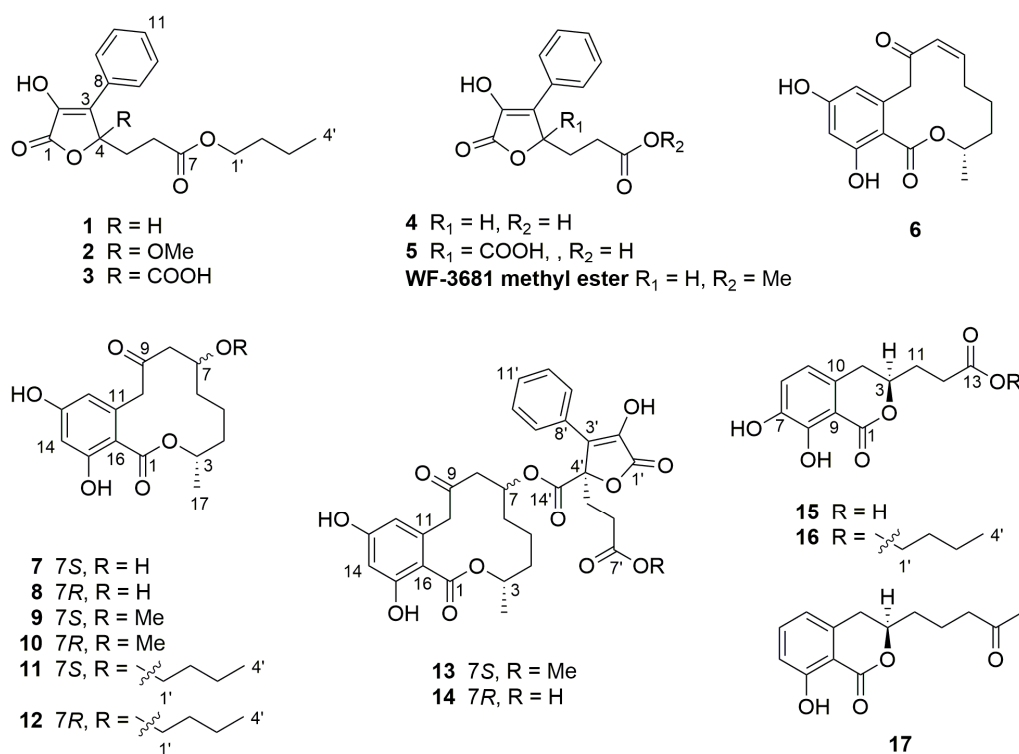


Figure 1. Structures of the compounds isolated from *Talaromyces rugulosus*.

2. Results

2.1. Structure Elucidation

Compound 1 was isolated as a brown amorphous solid. It has the molecular formula C₁₇H₂₀O₅ as determined by ESI-HRMS (ElectroSpray Ionization-High Resolution Mass Spectrometry) corresponding to eight degrees of unsaturation. Its UV absorbances at λ_{max} 207, 218 and 288 nm were similar to those of the co-isolated known butenolide derivative lactone acid (4) [13]. The NMR (Nuclear Magnetic Resonance) data of compound 1 (Table 1) were likewise comparable to those of 4 and included typical signals for a *mono*-substituted benzene ring at δ_H 7.75 (2H, d, J = 7.5 Hz, H-9 and H-13), 7.44 (2H, t, J = 7.5 Hz, H-10 and H-12) and 7.35 (1H, t, J = 7.5 Hz, H-11), an oxygenated methine proton at δ_H 5.52 (H-4), as well as two methylene groups at δ_H 2.45, 1.75 (H_{ab}-5) and 2.44 (H₂-6). The COSY (Correlation SpectroscopY) correlations between H-4/H₂-5 and H₂-5/H₂-6 together

with the HMBC (Heteronuclear Multiple Bond Correlation) correlations from H-4 to C-1 (δ_C 171.0), C-2 (δ_C 139.5), C-3 (δ_C 130.6) and C-8 (δ_C 131.9) and from H_{ab}-5 and H₂-6 to C-7 (δ_C 174.6) indicated that compound **1** shared the same core structure as **4**. In addition, signals of a methyl at δ_H 0.94 (Me-4') and three methylene groups at δ_H 1.38 (H₂-3'), 1.60 (H₂-2'), 4.08 (H-1'a) and 4.04 (H-1'b) were observed. The COSY correlations between Me-4'/H₂-3'/H₂-2'/H_{ab}-1' and the HMBC correlation from H_{ab}-1' to C-7 confirmed a *n*-butyl side chain to be attached to C-7 through an ester bond. Thus, the planar structure of **1** was elucidated as an unsaturated γ -lactone with propanoic acid *n*-butyl ester side chain. The absolute configuration of **1** was elucidated by comparing its experimental ECD spectrum with that of WF-3681 methyl ester [14], which can be considered a close analogue of **1**. Based on the good overall agreement, **1** has (*S*) absolute configuration.

Table 1. ¹H and ¹³C NMR (Nuclear Magnetic Resonance) Data for compounds **1**–**3**.

No.	1 ^a		2 ^a		3 ^a	
	δ_C , Type	δ_H (J in Hz)	δ_C , Type	δ_H (J in Hz)	δ_C , Type	δ_H (J in Hz)
1	171.0, C		168.3, C		170.0, C	
2	139.5, C		142.7, C		141.6, C	
3	130.6, C		124.6, C		128.7, C	
4	79.3, CH	5.52, dd (8.1, 2.2)	109.8, C		86.8, C	
5	30.5, CH ₂	2.45, m	34.6, CH ₂	2.54, ddd (14.5, 7.9, 6.5)	30.0, CH ₂	2.68, ddd (15.2, 8.7, 6.4)
		1.75, m		2.18, ddd (14.5, 7.9, 6.5)		2.48, ddd (15.2, 8.7, 6.4)
6	30.0, CH ₂	2.44, m	29.4, CH ₂	2.42, ddd (16.0, 7.9, 6.5)	29.1, CH ₂	2.25, ddd (15.8, 8.7, 6.4)
				2.31, ddd (16.0, 7.9, 6.5)		2.15, ddd (15.8, 8.7, 6.4)
7	174.6, C		174.5, C		174.2, C	
8	131.9, C		131.3, C		131.3, C	
9, 13	128.6, CH	7.75, d (7.5)	128.6, CH	7.93, d (7.5)	128.6, CH	7.76, d (7.4)
10, 12	129.7, CH	7.44, t (7.5)	129.8, CH	7.45, t (7.5)	129.7, CH	7.42, t (7.4)
11	129.7, CH	7.35, t (7.5)	129.8, CH	7.36, t (7.5)	129.9, CH	7.35, t (7.4)
14					171.9, C	
1'	65.6, CH ₂	4.08, dt (10.8, 6.6)	65.6, CH ₂	4.02, dt (10.8, 6.7)	65.7, CH ₂	4.00, dt (10.8, 6.7)
		4.04, dt (10.8, 6.6)		3.97, dt (10.8, 6.7)		3.94, dt (10.8, 6.7)
2'	31.7, CH ₂	1.60, m	31.7, CH ₂	1.56, m	31.6, CH ₂	1.54, m
3'	20.2, CH ₂	1.38, m	20.2, CH ₂	1.36, m	20.1, CH ₂	1.34, m
4'	14.0, CH ₃	0.94, t (7.3)	14.0, CH ₃	0.93, t (7.3)	14.0, CH ₃	0.91, t (7.3)
OMe-4			50.7, CH ₃	3.18, s		

^a Recorded at 300 MHz (¹H) and 75 MHz (¹³C) in CD₃OD.

The UV (UltraViolet) spectrum of compound **2** was similar to that of **1**. The ESI-HRMS data revealed the molecular formula C₁₈H₂₂O₆, suggesting the presence of an additional methoxy group in **2** compared to **1**, which was observed at δ_H 3.18 and δ_C 50.7, respectively. The disappearance of the oxygenated methine proton along with the HMBC correlation from the protons of the methoxy group to C-4 (δ_C 109.8) indicated this additional methoxy group to be located at the C-4 position. The remaining structure of **2** was elucidated to be identical to that of **1** as indicated by detailed analysis of the 2D NMR spectra of **2**. Thus, compound **2** was identified as 4-methoxylactone acid *n*-butyl ester. The ECD spectrum of **2** was rather weak and noisy, but similar to that of chaetobutenolide C [14], which can be used for ECD correlation and indicated a non-racemic mixture of (*R*) and (*S*) isomers with a slight excess of the (*R*) enantiomer.

The molecular formula of **3** was deduced as C₁₈H₂₀O₇ from ESI-HRMS data. The UV and NMR data (Table 1) of **3** resembled those of the co-isolated lactone diacid (**5**) [13], except for the observation

of an additional *n*-butyl chain as described for **1**. In the HMBC spectrum of **3**, H₂-5 (δ_{H} 2.68 and 2.48), H₂-6 (δ_{H} 2.25 and 2.15) and H₂-1' (δ_{H} 4.00 and 3.94) exhibited correlations to C-7 (δ_{C} 174.2) while only H₂-5 showed correlation to C-14 (δ_{C} 171.9), indicating the *O*-*n*-butyl group to be attached to C-7. Thus, compound **3** was elucidated as lactone diacid 7-*O*-*n*-butyl ester. Compound **3** decomposed before ECD measurements. Its absolute configuration can be tentatively assigned upon biosynthetic considerations as (*R*) similarly to **5**.

To elucidate the absolute configuration of the known natural product **5**, the solution TDDFT-ECD (Time-Dependent Density Functional Theory-Electronic Circular Dichroism) protocol was applied on the arbitrarily chosen (*R*) enantiomer [15,16]. Merck Molecular Force Field (MMFF) conformational search with an implicit solvent model for CHCl₃ resulted in 149 conformers in a 21 kJ/mol energy window. DFT reoptimization of these yielded 9, 12 and 12 low-energy ($\geq 2\%$) conformers at the B3LYP/6-31G(d) in vacuo, the B97D/TZVP PCM (Polarizable Continuum Model)/MeCN and the CAM-B3LYP/TZVP PCM/MeCN levels, respectively. Boltzmann-averaged ECD spectra of (*R*)-**5** resembled the experimental ECD spectrum allowing elucidation of the absolute configuration as (*R*) (Figure 2).

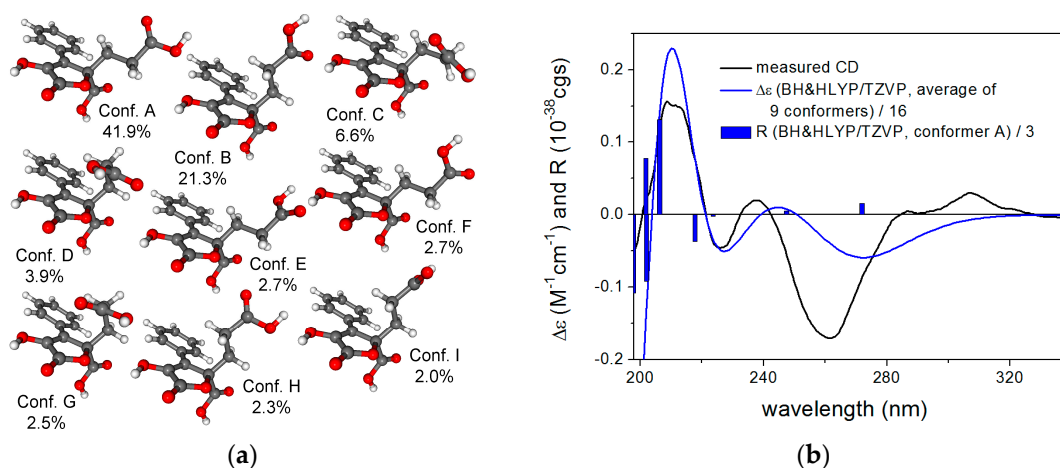


Figure 2. (a) structures and populations of the low-energy B3LYP/6-31G(d) in vacuo conformers ($\geq 2\%$) of (*R*)-**5**; (b) experimental ECD spectrum of **5** in MeCN compared with the Boltzmann-weighted BH&HLYP/TZVP ECD spectrum of (*R*)-**5** computed for the B3LYP/6-31G(d) in vacuo conformers. Bars represent the rotational strength values of the lowest-energy conformer.

The NMR data of compounds **6–10** were found to be identical to those of (*3R*)-*cis*-resorcylicide, (*3R,7R*)-7-hydroxyresorcylicide, (*3R,7S*)-7-hydroxyresorcylicide, (*3R,7R*)-7-methoxyresorcylicide and (*3R,7S*)-7-methoxyresorcylicide, respectively (Tables 2 and 3). These resorcylicides were first reported by Barrow et al. and the absolute configuration at C-3 was suggested to be *S* in consideration of their biosynthesis [17]. Later, it was revised to (*3R*) by chemical derivatization, ECD calculation and X-ray diffraction analysis [18–20]. However, the resorcylicides isolated in this study exhibited mirror-imaged CD (Circular dichroism) curves compared to those of the corresponding compounds found in the literature, indicating that they should be enantiomers of the previously reported resorcylicide derivatives and possess *3S* configuration. The above-mentioned TDDFT-ECD protocol was carried out on the arbitrarily chosen (*R*) enantiomer of **6** yielding 33 MMFF conformers, and 7 and 12 low-energy conformers at the B3LYP/6-31G(d) and the B97D/TZVP levels. Boltzmann averaged ECD spectra computed for both sets of conformers gave mirror-image agreement with the experimental spectrum, allowing elucidation of the absolute configuration as (*S*) in line with the literature (Figure 3).

Table 2. ^1H and ^{13}C NMR Data for compounds 6–8.

No.	6 ^a		7 ^b		8 ^b	
	δ_{C} , Type	δ_{H} (J in Hz)	δ_{C} , Type ^c	δ_{H} (J in Hz)	δ_{C} , Type ^c	δ_{H} (J in Hz)
1	172.9, C		n.d. ^d		n.d. ^d	
3	76.9, CH	5.03, m	75.5, CH	4.95, m	73.1, CH	5.19, m
4	32.2, CH ₂	1.87, m	33.1, CH ₂	1.91, m	32.9, CH ₂	1.68, m
		1.65, m		1.75, m		
5	26.4, CH ₂	1.68, m	21.5, CH ₂	1.70, m	18.9, CH ₂	1.58, m
				1.43, m		
6	27.6, CH ₂	2.52, m	36.5, CH ₂	1.58, m	36.8, CH ₂	1.81, m
		2.21, m				1.50, m
		5.81, ddd				
7	139.9, CH	(11.8, 10.0, 5.7)	66.2, CH	4.39, m	66.9, CH	4.36, m
8	132.8, CH	6.51, br d (11.8)	53.5, CH ₂	3.03, dd (13.0, 3.1)	51.3, CH ₂	2.94, dd (15.4, 10.1)
				2.42, dd (13.0, 10.3)		2.61, dd (15.4, 1.6)
9	204.7, C		206.3, C		205.2, C	
10	51.5, CH ₂	4.58, d (18.4)	50.2, CH ₂	4.84, d (18.4)	52.3, CH ₂	4.59, d (18.5)
		3.65, d (18.4)		3.75, d (18.4)		3.90, d (18.5)
11	140.1, C		140.0, C		140.2, C	
12	113.9, CH	6.16, d (2.5)	113.5, CH	6.23, d (2.5)	113.2, CH	6.23, d (2.5)
13	164.1, C		162.7, C		162.9, C	
14	103.0, CH	6.26, d (2.5)	102.2, CH	6.31, d (2.5)	102.3, CH	6.32, d (2.5)
15	167.1, C		165.5, C		166.4, C	
16	106.2, C		106.3, C		105.6, C	
17	21.5, CH ₃	1.28, d (6.2)	20.9, CH ₃	1.31, d (6.1)	18.2, CH ₃	1.29, d (6.4)

7-OMe

^a Recorded at 600 MHz (^1H) and 150 MHz (^{13}C) in CD_3OD . ^b Recorded at 600 MHz (^1H) and 150 MHz (^{13}C) in CD_3COCD_3 . ^c Data extracted from HSQC (Heteronuclear Single Quantum Correlation) and HMBC. ^d n.d. = not detected.

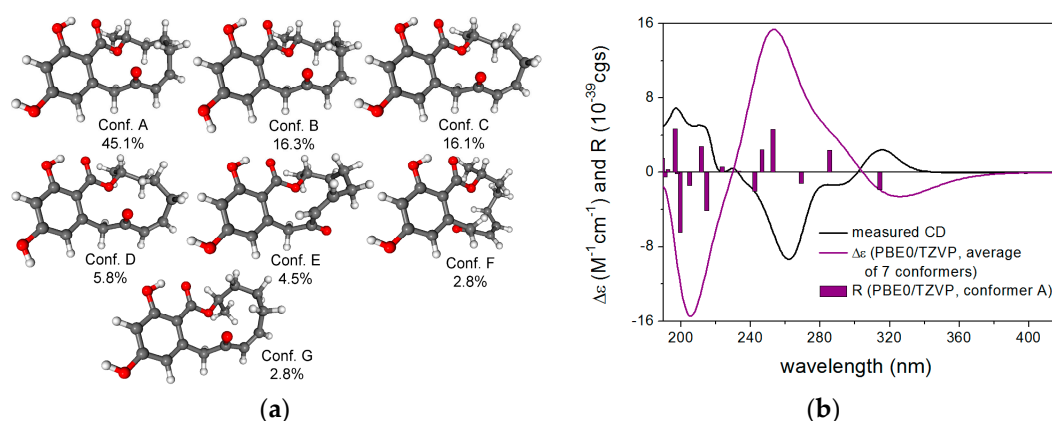


Figure 3. (a) structures and populations of the low-energy B3LYP/6-31G(d) in vacuo conformers ($\geq 2\%$) of (*R*)-6; (b) experimental ECD spectrum of 6 in MeCN compared with the Boltzmann-weighted PBE0/TZVP ECD spectrum of (*R*)-6 computed for the B3LYP/6-31G(d) in vacuo conformers. Bars represent the rotational strength values of the lowest-energy conformer.

Similar ECD pattern was observed in the experimental ECD spectrum of 9, and good agreement of the experimental and TDDFT-ECD spectra allowed determining the absolute configuration as (3*S*,7*S*)-9 (Figure S92). The calculations also confirmed that the stereochemistry of the C-3 lactone carbon has dominant contribution to the ECD spectra. Thus, compounds 6–10

are determined as (3*S*)-*cis*-resorcylicide, (3*S*,7*S*)-7-hydroxyresorcylicide, (3*S*,7*R*)-7-hydroxyresorcylicide, (3*S*,7*S*)-7-methoxy-resorcylicide and (3*S*,7*R*)-7-methoxyresorcylicide, respectively.

Table 3. ^1H and ^{13}C NMR Data for compounds **9** and **10**.

No.	9 ^a		10 ^a	
	δ_{C} , Type	δ_{H} (J in Hz)	δ_{C} , Type	δ_{H} (J in Hz)
1	172.5, C		172.3, C	
3	76.1, CH	4.93, m	73.8, CH	5.19, m
4	33.8, CH ₂	1.82, m 1.75, m	33.5, CH ₂	1.63, m
5	21.7, CH ₂	1.68, m 1.40, m	19.0, CH ₂	1.58, m
6	34.4, CH ₂	1.69, m 1.50, m	34.0, CH ₂	1.87, m 1.49, m
7	77.1, CH	3.95, m	78.2, CH	3.90, m
8	49.6, CH ₂	3.10, dd (13.3, 2.8) 2.40, dd (13.3, 10.2)	47.4, CH ₂	2.89, dd (15.7, 9.7) 2.71, dd (15.7, 1.0)
9	208.8, C		208.1, C	
10	51.0, CH ₂	4.68, d (18.7) 3.80, d (18.7)	53.2, CH ₂	4.63, d (18.8) 3.84, d (18.8)
11	139.6, C		139.9, C	
12	113.9, CH	6.14, d (2.5)	113.7, CH	6.13, d (2.5)
13	163.7, C		163.9, C	
14	102.9, CH	6.25, d (2.5)	103.0, CH	6.25, d (2.5)
15	166.0, C		166.9, C	
16	107.0, C		106.4, C	
17	21.1, CH ₃	1.32, d (6.1)	18.5, CH ₃	1.29, d (6.4)
7-OMe	56.7, CH ₃	3.42, s	56.5, CH ₃	3.34, s

^a Recorded at 600 MHz (^1H) and 150 MHz (^{13}C) in CD₃OD.

Based on ESI-HRMS data, the molecular formula of compound **11** was determined to be C₂₀H₂₈O₆, containing an additional C₄H₈ unit when compared to **7**. Comparison of the ^1H and ^{13}C NMR data of **7** and **11** (Table 4) revealed the existence of an additional *n*-butyl group in **11**, which is further confirmed by the COSY correlations between Me-4' (δ_{H} 0.95)/H₂-3' (δ_{H} 1.42), H₂-3'/H₂-2' (δ_{H} 1.56), H₂-2'/H_a-1' (δ_{H} 3.63) and H₂-2'/H_b-1' (δ_{H} 3.51). Examination of the 2D NMR spectra of **11** indicated it to share the same resorcylicide ring structure as found in compounds **7–10**. Key HMBC correlations from H_{ab}-1' to C-7 (δ_{C} 75.4) and from H-7 (δ_{H} 4.04) to C-1' (δ_{C} 69.7) confirmed the linkage between C-7 and the additional *n*-butyl group via an ether bond in **11**. Thus, the planar structure of **11** was elucidated as 7-*O-n*-butylresorcylicide. Compound **12** shared the same gross structure as **11** as confirmed by 2D NMR and ESI-HRMS data. The structural difference between **11** and **12** is confined to the configuration at C-7 as already found for **7** and **8**, and for **9** and **10**. Comparison of the NMR data of **11** and **12**, especially of the coupling constants between H-7 and H_{ab}-8 and of the chemical shifts of C-3, H-3 and C-17 (Table 5), indicated that **11** shared the same relative configuration as **7** and **9**, whereas **12** shared the same relative configuration as **8** and **10**. Moreover, the CD data of **11** were comparable to those of **7** and **9**, whereas the ECD data of **12** resembled those of **8** and **10**. The above findings revealed compounds **11** and **12** to be (3*S*,7*S*)-7-*O-n*-butylresorcylicide and (3*S*,7*R*)-7-*O-n*-butylresorcylicide, respectively.

Table 4. ^1H and ^{13}C NMR Data for compounds **11** and **12**.

No.	11 ^a		12 ^b	
	δ_{C} , Type	δ_{H} (J in Hz)	δ_{C} , Type	δ_{H} (J in Hz)
1	172.5, C		172.3, C	
3	76.2, CH	4.94, m	73.9, CH	5.19, m
4	33.8, CH ₂	1.80, m	33.6, CH ₂	1.64, m
5	21.9, CH ₂	1.75, m	19.1, CH ₂	1.58, m
		1.69, m		
6	34.6, CH ₂	1.40, m	34.3, CH ₂	1.84, m
		1.66, m		
7	75.4, CH	1.50, m	76.5, CH	1.51, m
		4.04, m		
8	50.3, CH ₂	3.09, dd (13.2, 3.0)	48.2, CH ₂	2.90, dd (15.6, 9.8)
		2.40, dd (13.2, 10.3)		
9	208.9, C		208.3, C	
10	50.9, CH ₂	4.69, d (18.7)	53.1, CH ₂	4.61, d (18.8)
		3.78, d (18.7)		
11	139.6, C		139.9, C	
12	114.0, CH	6.13, d (2.5)	113.8, CH	6.12, d (2.5)
13	163.7, C		163.9, C	
14	102.9, CH	6.25, d (2.5)	103.1, CH	6.25, d (2.5)
15	166.0, C		166.8, C	
16	107.0, C		106.5, C	
17	21.1, CH ₃	1.31, d (6.1)	18.6, CH ₃	1.29, d (6.4)
1'	69.7, CH ₂	3.63, dt (9.2, 6.4)	69.5, CH ₂	3.51, dt (9.3, 6.5)
		3.51, dt (9.2, 6.4)		
2'	33.2, CH ₂	1.56, m	33.2, CH ₂	1.53, m
3'	20.4, CH ₂	1.42, m	20.4, CH ₂	1.38, m
4'	14.3, CH ₃	0.95, t (7.3)	14.2, CH ₃	0.93, t (7.3)

^a Recorded at 300 MHz (^1H) and 75 MHz (^{13}C) in CD_3OD . ^b Recorded at 500 MHz (^1H) and 125 MHz (^{13}C) in CD_3OD .

Table 5. Key differences of NMR Data for compounds **7–14**.

Compounds	7	9	11	13	8	10	12	14
$^3J_{7,8a}$ (Hz)	3.1	2.8	3.0	3.1	10.1	9.6	9.8	10.4
$^3J_{7,8b}$ (Hz)	10.3	10.2	10.3	10.4	1.6	1.0	1.0	- ^a
C-3	75.5	76.1	76.2	76.1	73.1	73.8	73.9	74.0
H-3	4.95	4.93	4.94	4.93	5.19	5.19	5.19	5.13
C-17	20.9	21.1	21.1	20.9	18.2	18.5	18.6	18.9

^a Signals overlapped.

Compound **13** was isolated as a brown amorphous solid. Its molecular formula was established as $\text{C}_{31}\text{H}_{32}\text{O}_{12}$ from ESI-HRMS data. Interestingly, the ^1H and ^{13}C NMR spectra of **13** (Table 6) showed two sets of signals corresponding to the macrolide (3*R*,7*R*)-7-hydroxyresorcylic acid (7) and the butenolide lactone diacid (5), which were co-isolated in the present study. For example, the two *meta*-coupling aromatic protons at δ_{H} 6.26 (d, $J = 2.5$ Hz, H-14) and 6.14 (d, $J = 2.5$ Hz, H-12), the two oxygenated methine protons at δ_{H} 5.54 (m, H-7) and 4.93 (m, H-3), the isolated methylene protons at δ_{H} 4.67 (d, $J = 18.8$ Hz, H_a-10) and 3.78 (d, $J = 18.8$ Hz, H_b-10) and the doublet methyl at δ_{H} 1.28 (d, $J = 6.2$ Hz, Me-17) represented characteristic signals for 7-hydroxyresorcylic acid. On the other side, signals of the *mono*-substituted benzene ring at δ_{H} 7.73 (d, $J = 7.7$ Hz, H-9' and H-13'), 7.44 (2H, t, $J = 7.7$ Hz, H-10' and H-12') and 7.37 (1H, t, $J = 7.7$ Hz, H-11') along with those of two methylene groups at δ_{H} 2.77, 2.59 (H_{ab}-5') and 2.29, 2.22 (H_{ab}-6') indicated the butenolide lactone diacid (5).

Table 6. ^1H and ^{13}C NMR Data for compounds **13** and **14**.

No.	13 ^a		14 ^a	
	δ_{C} , Type	δ_{H} (J in Hz)	δ_{C} , Type	δ_{H} (J in Hz)
1	172.4, C		172.2, C	
3	76.1, CH	4.93, m	74.0, CH	5.13, m
4	33.4, CH ₂	1.75, m 1.61, m	33.8, CH ₂	1.66, m
5	21.2, CH ₂	1.39, m 1.31, m	19.0, CH ₂	1.52, m
6	33.2, CH ₂	1.57, m	32.8, CH ₂	1.84, m 1.56, m
7	72.9, CH	5.54, m	74.2, CH	5.53, m
8	49.2, CH ₂	2.94, dd (13.3, 3.1) 2.58, dd (13.3, 10.4)	46.9, CH ₂	3.07, dd (15.8, 10.4) 2.49, d (15.8)
9	206.6, C		206.1, C	
10	50.8, CH ₂	4.67, d (18.8) 3.78, d (18.8)	52.8, CH ₂	4.52, d (18.8) 3.73, d (18.8)
11	139.3, C		139.6, C	
12	114.1, CH	6.14, d (2.4)	113.8, CH	6.07, d (2.5)
13	163.8, C		163.9, C	
14	103.0, CH	6.26, d (2.4)	103.0, CH	6.24, d (2.5)
15	166.2, C		166.8, C	
16	106.7, C		106.2, C	
17	20.9, CH ₃	1.28, d (6.2)	18.9, CH ₃	1.27, d (6.4)
1'	169.8, C		169.7, C	
2'	141.9, C		141.8, C	
3'	128.1, C		128.6, C	
4'	86.6, C		86.6, CH	
5'	30.1, CH ₂	2.77, ddd (15.2, 8.6, 6.4) 2.59, ddd (15.2, 8.6, 6.4)	30.0, CH ₂	2.72, ddd (15.3, 8.7, 6.5) 2.49, ddd (15.3, 8.7, 6.5)
6'	28.7, CH ₂	2.29, ddd (16.0, 8.6, 6.4) 2.22, ddd (16.0, 8.6, 6.4)	28.7, CH ₂	2.23, ddd (15.9, 8.7, 6.5) 2.14, ddd (15.9, 8.7, 6.5)
7'	174.4, C		175.9, C	
8'	131.0, C		131.0, C	
9', 13'	128.6, CH	7.73, d (7.7)	128.5, CH	7.70, d (7.4)
10', 12'	129.9, CH	7.44, t (7.7)	129.9, CH	7.44, t (7.4)
11'	130.1, CH	7.37, t (7.7)	130.1, CH	7.37, t (7.4)
14'	169.9, C		169.5, C	
OMe	52.3, C	3.58, s		

^a Recorded at 700 MHz (^1H) and 175 MHz (^{13}C) in CD₃OD.

Detailed analysis of the 2D NMR spectra of **13** established the two subunits of resorcylic acid and butenolide as shown. The HMBC correlations from H-7 and H_{ab}-5' to C-14' (δ_{C} 169.9) indicated the connection of these two subunits through the C(7)-O-C(14') ester bond. In addition, the attachment of a methoxy group (δ_{H} 3.58 and δ_{C} 52.3) at C-7' was deduced by the HMBC correlation from the protons of the methoxy group to C-7' (δ_{C} 174.4). Thus, the structure of compound **13** was elucidated as shown, representing a butenolide-resorcylic acid dimer, for which the name talarodilactone A is proposed. Comparison of its NMR data with those of other resorcylic acid derivatives (Table 5) indicated that compound **13** shared the same relative configuration as **7**, **9** and **11** regarding the macrolactone part. The ECD spectrum of **13** was found to be similar to those of resorcylic acid monomers, which suggested that the ECD spectrum of **13** is mainly governed by the C-3 chiral center of the resorcylic acid moiety and thus the absolute configuration of this chiral center could be unambiguously elucidated as (3*S*). On the basis of the (3*S**,7*S**) relative configuration determined by NMR experiments, the absolute configuration of the RAL subunit of **13** was determined as (3*S*,7*S*). Considering the shape of the ECD spectrum of **13**, it more resembles those of **7** and **9** than those of **8** and **10** supporting the assignment of

C-7 as (S). The absolute configuration of the butenolide part can be tentatively assigned as (R) on the basis of biosynthetic considerations.

The molecular formula of compound **14** was determined to be C₃₀H₃₀O₁₂, suggesting the loss of one methoxy group compared to **13**, which was confirmed by the disappearance of the respective signal in the NMR spectra of **14**. Furthermore, comparison of the NMR data of **14** with those of the other resorcylic derivatives isolated in this study (Table 5) revealed that **14** shared the same relative configuration as **8**, **10** and **12** at C-3 and C-7. Similarly to **13**, the (3S) absolute configuration of **14** can be unambiguously deduced from the ECD spectrum, while that of C-7 can be determined as (R) by utilizing the experimental NMR data. The C-4' chiral center can be only tentatively assigned as (R) on the basis of biosynthetic considerations.

Compound **15** was isolated as a brown amorphous solid, exhibiting UV absorbance maxima at 220, 258 and 334 nm. Its molecular formula was found to be C₁₂H₁₂O₆ as confirmed by ESI-HRMS data, indicating seven degrees of unsaturation. The ¹H NMR spectrum of **15** (Table 7) showed two *ortho*-coupling protons at δ_H 7.01 (d, J = 8.0 Hz, H-6) and 6.63 (d, J = 8.0 Hz, H-5), suggesting the presence of a 1,2,3,4-tetrasubstituted benzene ring. A spin system containing an oxygenated methine at δ_H 4.63 (H-3) and three aliphatic methylenes at δ_H 2.94 and 2.83 (H_{ab}-4), 1.96 (H₂-11) and 2.42 (H₂-12) was identified by their COSY correlations. In addition, three hydroxy groups at δ_H 12.21 (s, OH-13), 10.82 (s, OH-8) and 9.33 (s, OH-7) were observed. The HMBC correlations from H-5 to C-7 (δ_C 144.4) and C-9 (δ_C 108.4), from H-6 to C-8 (δ_C 149.9) and C-10 (δ_C 129.1), from OH-7 to C-6 (δ_C 121.6), C-7 and C-8, and from OH-8 to C-7, C-8 and C-9 established a benzene ring with two hydroxy groups at C-7 and C-8. The HMBC correlations from H-5 to C-4 (δ_C 31.2), from H_{ab}-4 to C-5 (δ_C 117.5), C-9 and C-10 as well as from H₂-11 and H₂-12 to C-13 (δ_C 173.8) indicated a 5-carboxypentyl chain to be attached at the C-10 position. Furthermore, the presence of an additional six-membered lactone ring fused with the benzene ring was confirmed by the HMBC correlations from H-5 and H-3 to C-1 (δ_C 169.6) combined with its molecular formula. The above findings concluded the structure of **15** as a new dihydroisocoumarin derivative as shown, for which the trivial name talumarin A is proposed.

Table 7. ¹H and ¹³C NMR Data for compounds **15** and **16**.

No.	15 ^a		16 ^b	
	δ _C , Type	δ _H (J in Hz)	δ _C , Type	δ _H (J in Hz)
1	169.6, C		169.5, C	
3	79.3, CH	4.63, m	80.8, CH	4.63, m
4	31.2, CH ₂	2.94, dd (16.4, 3.6) 2.83, dd (16.4, 10.9)	32.7, CH ₂	2.96, dd (16.1, 4.1) 2.87, dd (16.1, 10.4)
5	117.5, CH	6.63, d (8.0)	118.6, CH	6.65, d (8.0)
6	121.6, CH	7.01, d (8.0)	122.4, CH	7.01, d (8.0)
7	144.4, C		145.7, C	
8	149.9, C		151.0, C	
9	108.4, C		109.4, C	
10	129.1, C		130.7, C	
11	29.3, CH ₂	1.96, m	30.7, CH ₂	2.09, m
12	29.1, CH ₂	2.42, m	30.3, CH ₂	2.58, m
13	173.8, C		174.4, C	
1'			65.3, CH ₂	4.11, t (6.6)
2'			31.6, CH ₂	1.63, m
3'			19.9, CH ₂	1.40, m
4'			13.7, CH ₃	0.95, t (7.4)
OH-7		9.33, s		
OH-8		10.82, s		
OH-13		12.21, s		

^a Recorded at 300 MHz (¹H) and 75 MHz (¹³C) in DMSO-*d*₆. ^b Recorded at 300 MHz (¹H) and 75 MHz (¹³C) in CD₃OD.

Compound **16** shares almost identical UV absorptions with **15**, suggesting the dihydroisocoumarin nature of the latter. The ESI-HRMS data established the molecular formula $C_{16}H_{20}O_6$ for **16**. The NMR data of **16** were likewise similar to those of **15** (Table 7). However, signals of an additional *n*-butyl moiety were observed in the NMR spectra of **16**, which was further confirmed by the COSY correlations between Me-4' (δ_H 0.95)/H₂-3' (δ_H 1.40), H₂-3'/H₂-2' (δ_H 1.63), and H₂-2'/H₂-1' (δ_H 4.11). In the HMBC spectrum, H₂-1' showed correlation to C-12 (δ_C 174.4), indicating the attachment of the *n*-butyl moiety to C-12 through an ester bond. The remaining structure of **16** was found to be identical to that of **15** by detailed analysis of the 2D NMR data of **16**.

To elucidate the absolute configuration of **15** and **16**, TDDFT-ECD calculations were performed on a truncated model compound of **16** (R = Me). MMFF conformational search of the (*R*) enantiomer resulted in 42 conformers in a 21 kJ/mol energy window—DFT reoptimization of which yielded 8, 18 and 12 low-energy conformers at the B3LYP/6-31G(d) in vacuo, the B97D/TZVP PCM/MeCN and the CAM-B3LYP/TZVP PCM/MeCN levels. ECD calculations performed for each set of conformers gave moderate to good overall agreement with the experimental spectra of **15** and **16**, allowing elucidation of the absolute configuration of **15** and **16** as (*R*) (Figure 4). The result of the ECD calculation corroborated with the previous ECD studies of the dihydroisocoumarin chromophore well [21–23], which located the $n\text{-}\pi^*$ ECD transition in the range of 250–270 nm and correlated the *P/M* helicity of the condensed heteroring with *positive/negative* $n\text{-}\pi^*$ Cotton effect, respectively. In the case of **15** and **16**, the heteroring adopts *M* helicity with equatorial C-3 substituent, which gives rise to a negative $n\text{-}\pi^*$ Cotton effect at 263 and 262 nm, respectively.

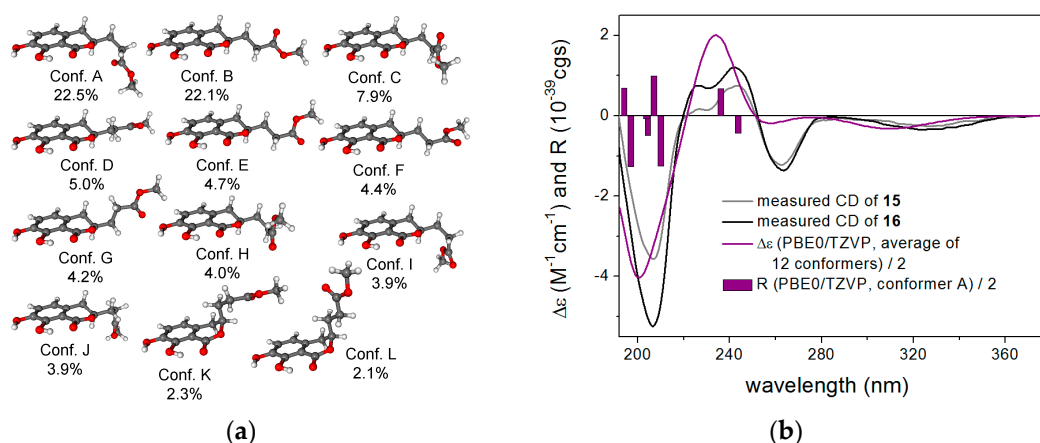


Figure 4. (a) structures and populations of the low-energy CAM-B3LYP/TZVP PCM/MeCN conformers ($\geq 2\%$) of the truncated model compound of (*R*)-**16**; (b) experimental ECD spectra of **15** and **16** in MeCN compared with the Boltzmann-weighted PBE0/TZVP PCM/MeCN ECD spectrum of the truncated model compound of (*R*)-**16** computed for the CAM-B3LYP/TZVP PCM/MeCN conformers. Bars represent the rotational strength values of the lowest-energy conformer.

The remaining known compounds were identified as lactone acid (**4**) [13], lactone diacid (**5**) [13], and aspergillumarin A (**17**) by comparison of their spectroscopic data with those in the literature [24,25].

2.2. Biological Activities

All isolated compounds (**1**–**17**) were evaluated for their cytotoxic activity against the L5178Y mouse lymphoma cell line. Only the two butenolide-resorcylic dimers talarodilactones A and B (**13** and **14**) exhibited potent cytotoxicity with IC₅₀ (half maximal Inhibitory Concentration) values of 3.9 and 1.3 μ M, respectively. Interestingly, the monomeric building blocks of **13** and **14**, which were also isolated in this study, were inactive in comparison.

Moreover, all compounds were tested for their antimicrobial activities against *Mycobacterium tuberculosis* (H37Rv), *Staphylococcus aureus* (ATCC 25923) and *Acinetobacter baumannii* (ATCC BAA-1605) using a broth micro dilution assay. However, none of them was active at a dose of 25 µg/mL.

3. Discussion

In conclusion, analysis of the sponge-derived fungus *T. rugulosus* afforded seventeen lactone derivatives divided into four groups: five butenolides (1–5), seven resorcylic derivatives (6–12), two butenolide-resorcylic dimers (13 and 14) and three dihydroisocoumarins (15–17). Compounds 1–3, 11, 12 and 16 exhibited a butyl side chain in their structures. Many butylated natural products have been isolated from fungi [26–28] and plants [29,30]. In our study, all butylated derivatives were clearly detected in the original crude fungal extract by LC-MS. Moreover, the extraction and isolation processes did not involve *n*-BuOH. After incubation of the corresponding non-butylated compounds with *n*-BuOH for one week, no butylation of these compounds was detected by LC-MS. These results confirm that the butylated compounds isolated in the present study are natural compounds.

Numerous (3*R*)-resorcylic derivatives have been reported [17–20]. Some of them that were initially presumed to possess 3*S* configuration were later revised to have 3*R* configuration instead. However, all resorcylic derivatives (6–14) isolated in the present study were unambiguously assigned as (3*S*)-series by CD analysis. To the best of our knowledge, this is the first report of (3*S*)-resorcylic derivatives in nature. In addition, talarodilactones A and B (13 and 14) represent a new class of butenolide-resorcylic dimers that showed significant cytotoxicity against the L5178Y murine lymphoma cell line with IC₅₀ values of 3.9 and 1.3 µM, respectively.

4. Materials and Methods

4.1. General Experimental Procedures

Optical rotations were measured using a PerkinElmer-241 MC polarimeter (Waltham, MA, USA). Bruker AVANCE DMX 300 or 600 NMR spectrometers (Karlsruhe, Germany) were employed to record ¹H, ¹³C and 2D NMR spectra. A Thermo Finnigan LCQ Deca LC-MS system (San Jose, CA, USA) was used to analyze the crude extract. ESI-HRMS data were obtained by a FT-HRMS-Orbitrap (Thermo Finnigan, San Jose, CA, USA) mass spectrometer. A Dionex P580 system (Germering, Germany) coupled to a photodiode array detector (UVD340S) was used to perform HPLC analysis. A Europhere 10 C₁₈ (125 × 4 mm, L × ID, Knauer, Germany) was used for analytical separation. HPLC separation was carried out with a Lachrom-Merck Hitachi semi-preparative HPLC system (Darmstadt, Germany) (Pump L7100; UV detector L7400; column: Europhere 100 C₁₈, 300 × 8 mm, Knauer, Germany). Merck MN silica gel 60 M (0.04–0.063 mm, Dueren, Germany) or Sephadex LH-20 (Darmstadt, Germany) were applied for column chromatography as stationary phases. Pre-coated silica gel 60 F₂₅₄ plates (Merck) were used for TLC (Thin layer chromatography) analysis under detection at 254 and 366 nm and/or using anisaldehyde as spray-reagent. Spectral grade solvents were used for spectroscopic measurements while distilled solvents were used for column chromatographic separations. ECD spectra were recorded on a J-810 spectropolarimeter.

4.2. Fungal Material

The fungal strain was isolated from the healthy inner tissues of the sponge *A. cannabina* collected and identified by Semih Engin at Sığaçık-İzmir, Turkey. It was identified as *Talaromyces rugulosus* (GenBank accession No. KT071708) according to DNA amplification and sequencing of the fungal ITS region as described before [31].

4.3. Fermentation, Extraction and Isolation

The fungal strain was cultivated on solid rice medium in twelve 1L Erlenmeyer flasks (autoclaving 100 g of rice and 110 mL of 3.5% sea salt solution in each Erlenmeyer flask) at room temperature under static conditions. After 30 d, each flask was extracted overnight with ethyl acetate (3×400 mL), followed by filtration and evaporation. The obtained crude extract (5 g) was then partitioned between *n*-hexane and 90% aqueous MeOH. The MeOH extract was then subjected to vacuum liquid chromatography (VLC) on silica gel 60 using a gradient solvent elution system of *n*-hexane/EtOAc and $\text{CH}_2\text{Cl}_2/\text{MeOH}$ to obtain 16 fractions (Fr.1 to Fr.16).

Fr.4 (509 mg) was fractionated on a Sephadex LH-20 column using MeOH as eluent to give ten subfractions (Fr.4-1 to Fr.4-10), among which subfraction Fr.4-6 was found to be the pure compound **6** (14.0 mg). Subfraction Fr.4-5 (119 mg) was further purified by semi-preparative HPLC with 60% MeOH/ H_2O as eluting system to afford **1** (9.9 mg), **11** (2.1 mg), **12** (2.5 mg) and **16** (2.0 mg).

Fr.5 (2.4 g) was subjected to a Sephadex LH-20 column with MeOH as mobile phase to yield nine subfractions (Fr.5-1 to Fr.5-9). Compounds **14** (3.9 mg) and **15** (3.1 mg) were obtained from subfraction Fr.5-6 (50.5 mg) by semi-preparative HPLC with a gradient of MeOH/ H_2O as eluent. Subfraction Fr.5-4 (570 mg) was chromatographed over a Sephadex LH-20 column using acetone to afford eight subfractions (Fr.5-4-1 to Fr.5-4-8). After purification by semi-preparative RP (Reversed Phase)-HPLC using a gradient elution of MeOH/ H_2O , subfractions Fr.5-4-5 (18.9 mg) and Fr.5-4-6 (13.1 mg) yielded compounds **8** (1.2 mg) and **4** (6.2 mg), respectively. Subfraction Fr.5-3 (788 mg) was fractionated over a Sephadex LH-20 column using MeOH as eluent to give five subfractions (Fr.5-3-1 to Fr.5-3-5). Subfraction Fr.5-3-2 (47.2 mg) was purified by semi-preparative RP-HPLC using a gradient elution of MeOH/ H_2O to yield **17** (9.3 mg). Following the same procedure as described for Fr.5-3-2, compounds **2** (2.2 mg), **3** (16.7 mg) and **5** (2.4 mg) were obtained from Fr.5-3-3 (71.5 mg) while compounds **7** (1.8 mg), **9** (1.5 mg), **10** (1.4 mg) and **13** (1.6 mg) were obtained from Fr.5-3-4 (53.7 mg).

Lactone acid n-butyl ester (1): brown amorphous solid; $[\alpha]_{\text{D}}^{23} +2$ (*c* 0.54, EtOH); UV λ_{max} 207, 217 and 288 nm; ECD {MeCN, λ [nm] ($\Delta\epsilon$), *c* = 3.29×10^{-4} M} 281 (+0.30), 231sh (−0.07); ^1H and ^{13}C NMR, see Table 1; ESI-HRMS *m/z* 327.1206 [M + Na]⁺ (calcd. for $\text{C}_{17}\text{H}_{20}\text{O}_5\text{Na}$, 327.1203).

4-Methoxylactone acid n-butyl ester (2): brown amorphous solid; $[\alpha]_{\text{D}}^{23} -4$ (*c* 0.33, EtOH); UV λ_{max} 203, 220 and 292 nm; ECD {MeCN, λ [nm] ($\Delta\epsilon$), *c* = 2.47×10^{-4} M} 263 (−0.32), 222 (−0.76), 210 (+0.16); ^1H and ^{13}C NMR, see Table 1; ESI-HRMS *m/z* 357.1308 [M + Na]⁺ (calcd. for $\text{C}_{18}\text{H}_{22}\text{O}_6\text{Na}$, 357.1309).

Lactone diacid 7-O-n-butyl ester (3): brown amorphous solid; $[\alpha]_{\text{D}}^{23} -4$ (*c* 0.53, EtOH); UV λ_{max} 204, 220 and 292 nm; ^1H and ^{13}C NMR, see Table 1; ESI-HRMS *m/z* 371.1101 [M + Na]⁺ (calcd. for $\text{C}_{18}\text{H}_{20}\text{O}_7\text{Na}$, 371.1101).

Lactone diacid (5): brown amorphous solid; $[\alpha]_{\text{D}}^{23} -3$ (*c* 0.53, EtOH); UV λ_{max} 219 and 292 nm; ECD {MeCN, λ [nm] ($\Delta\epsilon$), *c* = 3.51×10^{-4} M} 307 (+0.03), 262 (−0.17), 238 (+0.02), 226 (−0.05), 209 (+0.16), 198 (−0.05); LC-MS *m/z* 315.0 [M + Na]⁺, 291.3 [M − H][−].

(3S)-cis-Resorcylicide (6): brown amorphous solid; $[\alpha]_{\text{D}}^{23} +2$ (*c* 0.10, MeOH); UV λ_{max} 216, 266 and 303 nm; ECD {MeCN, λ [nm] ($\Delta\epsilon$), *c* = 3.88×10^{-4} M} 316 (+2.41), 288sh (−1.37), 262 (−9.35), 230sh (+0.42), 211sh (+5.08), 198 (+6.90); ^1H and ^{13}C NMR, see Table 2; ESI-HRMS *m/z* 291.1233 [M + H]⁺ (calcd. for $\text{C}_{16}\text{H}_{19}\text{O}_5$, 291.1227).

(3S,7S)-7-Hydroxyresorcylicide (7): brown amorphous solid; $[\alpha]_{\text{D}}^{23} +18$ (*c* 0.11 MeOH); UV λ_{max} 212, 264 and 302 nm; ECD {MeCN, λ [nm] ($\Delta\epsilon$), *c* = 2.27×10^{-4} M} 306 (+1.11), 286sh (+0.15), 261 (−5.71), 228sh (−1.99), 212 (+5.82); ^1H and ^{13}C NMR, see Table 2; ESI-HRMS *m/z* 309.1333 [M + H]⁺ (calcd. for $\text{C}_{16}\text{H}_{21}\text{O}_6$, 309.1333).

(3S,7R)-7-Hydroxyresorcylicide (8): brown amorphous solid; $[\alpha]_{\text{D}}^{23} -8$ (*c* 0.13 MeOH); UV λ_{max} 213, 263 and 302 nm; ECD {MeCN, λ [nm] ($\Delta\epsilon$), *c* = 3.24×10^{-4} M} 308 (+0.28), 285sh (−0.54), 260 (−3.33),

228sh (−1.81), 211 (+5.46); ^1H and ^{13}C NMR, see Table 2; ESI-HRMS m/z 309.1327 $[\text{M} + \text{H}]^+$ (calcd. for $\text{C}_{16}\text{H}_{21}\text{O}_6$, 309.1333).

(3*S*,7*S*)-7-Methoxyresorcyllide (**9**): brown amorphous solid; $[\alpha]_{\text{D}}^{23} +4$ (c 0.13, MeOH); UV λ_{max} 213, 263 and 304 nm; ECD {MeCN, λ [nm] ($\Delta\epsilon$), $c = 3.72 \times 10^{-4}$ M} 302 (+1.62), 284sh (+0.78), 260 (−6.22), 228sh (−1.53), 212 (+3.34), 191 (−5.60); ^1H and ^{13}C NMR, see Table 3; ESI-HRMS m/z 323.1495 $[\text{M} + \text{H}]^+$ (calcd. for $\text{C}_{17}\text{H}_{23}\text{O}_6$, 323.1489).

(3*S*,7*R*)-7-Methoxyresorcyllide (**10**): brown amorphous solid; $[\alpha]_{\text{D}}^{23} -8$ (c 0.12, MeOH); UV λ_{max} 213, 265 and 298 nm; ECD {MeCN, λ [nm] ($\Delta\epsilon$), $c = 1.86 \times 10^{-4}$ M} 308 (+0.50), 287sh (−0.79), 260 (−5.47), 228sh (−2.77), 211 (+9.62); ^1H and ^{13}C NMR, see Table 3; ESI-HRMS m/z 323.1493 $[\text{M} + \text{H}]^+$ (calcd. for $\text{C}_{17}\text{H}_{23}\text{O}_6$, 323.1489).

(3*S*,7*S*)-7-*O*-*n*-Butylresorcyllide (**11**): brown amorphous solid; $[\alpha]_{\text{D}}^{23} +5$ (c 0.20, MeOH); UV λ_{max} 213, 265 and 303 nm; ECD {MeCN, λ [nm] ($\Delta\epsilon$), $c = 1.58 \times 10^{-4}$ M} 302 (+6.88), 284sh (+3.87), 261 (−21.91), 230sh (−5.75), 212 (+16.12), 191 (−22.28); ^1H and ^{13}C NMR, see Table 4; ESI-HRMS m/z 365.1964 $[\text{M} + \text{H}]^+$ (calcd. for $\text{C}_{20}\text{H}_{29}\text{O}_6$, 365.1959).

(3*S*,7*R*)-7-*O*-*n*-Butylresorcyllide (**12**): brown amorphous solid; $[\alpha]_{\text{D}}^{23} -17$ (c 0.20, MeOH); UV λ_{max} 213, 264 and 303 nm; ECD {MeCN, λ [nm] ($\Delta\epsilon$), $c = 2.88 \times 10^{-4}$ M} 309 (+0.23), 287sh (−0.74), 260 (−4.38), 227sh (−2.93), 210 (+8.23); ^1H and ^{13}C NMR, see Table 4; ESI-HRMS m/z 365.1961 $[\text{M} + \text{H}]^+$ (calcd. for $\text{C}_{20}\text{H}_{29}\text{O}_6$, 365.1959).

Talarodilactone A (**13**): brown amorphous solid; $[\alpha]_{\text{D}}^{23} +9$ (c 0.21, MeOH); UV λ_{max} 212, 269 and 291 nm; ECD {MeCN, λ [nm] ($\Delta\epsilon$), $c = 1.68 \times 10^{-4}$ M} 296sh (+1.05), 284 (+1.11), 260 (−4.22), 226sh (−1.51), 209 (+3.86); ^1H and ^{13}C NMR, see Table 6; ESI-HRMS m/z 619.1794 $[\text{M} + \text{Na}]^+$ (calcd. for $\text{C}_{31}\text{H}_{32}\text{O}_{12}\text{Na}$, 619.1786).

Talarodilactone B (**14**): brown amorphous solid; $[\alpha]_{\text{D}}^{23} -22$ (c 0.21, MeOH); UV λ_{max} 212, 268 and 291 nm; ECD {MeCN, λ [nm] ($\Delta\epsilon$), $c = 2.49 \times 10^{-4}$ M} 298 (+0.79), 285sh (+0.31), 259 (−5.69), 235 (+0.25), 225 (−4.24), 208 (+11.95); ^1H and ^{13}C NMR, see Table 6; ESI-HRMS m/z 605.1625 $[\text{M} + \text{Na}]^+$ (calcd. for $\text{C}_{30}\text{H}_{30}\text{O}_{12}\text{Na}$, 605.1629).

Talumarin A (**15**): brown amorphous solid; $[\alpha]_{\text{D}}^{23} -18$ (c 0.27, CHCl_3); UV λ_{max} 220, 258 and 334 nm; ECD {MeCN, λ [nm] ($\Delta\epsilon$), $c = 9.91 \times 10^{-5}$ M} 324 (−0.35), 263 (−1.36), 242 (+1.20), 226sh (+0.75), 207 (−5.24); ^1H and ^{13}C NMR, see Table 7; ESI-HRMS m/z 275.0528 $[\text{M} + \text{Na}]^+$ (calcd. for $\text{C}_{12}\text{H}_{12}\text{O}_6\text{Na}$, 275.0526).

Talumarin B (**16**): brown amorphous solid; $[\alpha]_{\text{D}}^{23} -32$ (c 0.27, CHCl_3); UV λ_{max} 221, 258 and 330 nm; ECD {MeCN, λ [nm] ($\Delta\epsilon$), $c = 7.09 \times 10^{-5}$ M} 327 (−0.26), 262 (−1.22), 243 (+0.75), 226sh (+0.17), 206 (−3.57); ^1H and ^{13}C NMR, see Table 7; ESI-HRMS m/z 331.1151 $[\text{M} + \text{Na}]^+$ (calcd. for $\text{C}_{16}\text{H}_{20}\text{O}_6\text{Na}$, 331.1151).

4.4. Computational Section

Geometry optimizations (B3LYP/6-31G(d) in vacuo, B97D/TZVP [32,33] and CAM-B3LYP/TZVP [34] with PCM solvent model for MeCN), and TDDFT calculations were performed with Gaussian 09 using various functionals (B3LYP, BH&HLYP, CAM-B3LYP and PBE0) and the TZVP basis set [35]. ECD spectra were generated as the sum of Gaussians with 2400 and 3000 cm^{-1} half-height width (corresponding to c.a. 14 and 17 nm at 240 nm), using dipole-velocity computed rotational strengths [36]. Mixed torsional/low mode conformational searches were carried out by means of the Macromodel 10.8.011 software (New York, NY, USA) using Merck Molecular Force Field (MMFF) with implicit solvent model for CHCl_3 applying a 21 kJ/mol energy window [37]. Boltzmann distributions were estimated from the B3LYP, B97D and CAM-B3LYP energies. In the case of the B3LYP/6-31G(d) in vacuo level, ZPVE corrections were applied. The MOLEKEL software package (New York, NY, USA) was used for visualization of the results [38].

4.5. Cytotoxicity Assay

Cytotoxicity against the L5178Y murine lymphoma cell line was tested using the MTT (3-(4,5-dimethylthiazol-2-yl)-2,5-diphenyltetrazolium bromide) method. The depsipeptide kahalalide F was used as positive control [39].

4.6. Antimicrobial Assay

The inoculum was obtained by direct colony suspension preparation. Antibacterial activities against *Mycobacterium tuberculosis* (H37Rv), *Staphylococcus aureus* (ATCC 25923) and *Acinetobacter baumannii* (ATCC BAA-1605) were evaluated by broth micro dilution methodology as stated by the recommendations of the Clinical and Laboratory Standards Institute (CLSI) [40].

Supplementary Materials: The following are available online at www.mdpi.com/1660-3397/15/11/359/s1, ESI-HRMS, 1D and 2D NMR spectra of all the new compounds as well as ECD spectra of compounds **1**, **2**, **5–16** and ECD calculations for compound **9**.

Acknowledgments: Peter Proksch wants to thank the Manchot Foundation and the DFG (GRK2158) for support. Tibor Kurtán and Attila Mándi thank the National Research, Development and Innovation Office (NKFI K120181 and PD121020) for financial support and the Governmental Information-Technology Development Agency (KIFÚ) for CPU time. We are grateful to Rainer Kalscheuer (University of Duesseldorf, Germany) for performing antimicrobial studies. Peter Proksch and Raha S. Orfali acknowledge support by the International Scientific Partnership Program of King Saud University (ISPP# 0065).

Author Contributions: Lisa Küppers and Weaam Ebrahim performed the experiments of extraction and isolation; Mona El-Neketi prepared the manuscript and contributed to part of the data analysis; Ferhat C. Özkaya and Weaam Ebrahim isolated, purified and identified the fungal strain; Attila Mándi and Tibor Kurtán performed the ECD calculations; Werner E. G. Müller carried out the cytotoxicity assay; Raha S. Orfali contributed to part of the data analysis; Rudolf Hartmann measured the 1D and 2D NMR spectra; Wenhan Lin and Weiguo Song contributed to part of the structure elucidation; Zhen Liu and Peter Proksch supervised the research work and revised the manuscript.

Conflicts of Interest: The authors declare no conflict of interest.

References

1. Hong, J.H.; Jang, S.; Heo, Y.M.; Min, M.; Lee, H.; Lee, Y.M.; Lee, H.; Kim, J.J. Investigation of marine-derived fungal diversity and their exploitable biological activities. *Mar. Drugs* **2015**, *13*, 4137–4155. [[CrossRef](#)] [[PubMed](#)]
2. Mayer, A.M.S.; Glaser, K.B.; Cuevas, C.; Jacobs, R.S.; Kem, W.; Little, R.D.; McIntosh, J.M.; Newman, D.J.; Potts, B.C.; Shuster, D.E. The odyssey of marine pharmaceuticals: A current pipeline perspective. *Trends Pharmacol. Sci.* **2010**, *31*, 255–265. [[CrossRef](#)] [[PubMed](#)]
3. Ebada, S.; Proksch, P. Marine-Derived Fungal Metabolites. In *Springer Handbook of Marine Biotechnology*; Springer: Berlin/Heidelberg, Germany, 2015; pp. 759–788.
4. Ebrahim, W.; El-Neketi, M.; Lewald, L.I.; Orfali, R.S.; Lin, W.; Rehberg, N.; Kalscheuer, R.; Daletos, G.; Proksch, P. Metabolites from the fungal endophyte *Aspergillus austroafricanus* in axenic culture and in fungal-bacterial mixed cultures. *J. Nat. Prod.* **2016**, *79*, 914–922. [[CrossRef](#)] [[PubMed](#)]
5. Liu, S.; Dai, H.; Makhoulfi, G.; Heering, C.; Janiak, C.; Hartmann, R.; Mándi, A.; Kurtán, T.; Müller, W.E.G.; Kassack, M.U.; et al. Cytotoxic 14-membered macrolides from a mangrove-derived endophytic fungus, *Pestalotiopsis microspora*. *J. Nat. Prod.* **2016**, *79*, 2332–2340. [[CrossRef](#)] [[PubMed](#)]
6. Elnaggar, M.S.; Ebada, S.S.; Ashour, M.L.; Ebrahim, W.; Müller, W.E.G.; Mándi, A.; Kurtán, T.; Singab, A.; Lin, W.; Liu, Z.; et al. Xanthenes and sesquiterpene derivatives from a marine-derived fungus *Scopulariopsis* sp. *Tetrahedron* **2016**, *72*, 2411–2419. [[CrossRef](#)]
7. Elnaggar, M.S.; Ebada, S.S.; Ashour, M.L.; Ebrahim, W.; Singab, A.; Lin, W.; Liu, Z.; Proksch, P. Two new triterpenoids and a new naphthoquinone derivative isolated from a hard coral-derived fungus *Scopulariopsis* sp. *Fitoterapia* **2017**, *116*, 126–130. [[CrossRef](#)] [[PubMed](#)]
8. Dong, Y.; Lin, J.; Lu, X.; Zheng, Z.; Ren, X.; Zhang, H.; He, J.; Yang, J. Cathepsin B inhibitory tetraene lactones from the fungus *Talaromyces wortmannii*. *Helv. Chim. Acta* **2009**, *92*, 567–574. [[CrossRef](#)]

9. Liu, F.; Cai, X.L.; Yang, H.; Xia, X.K.; Guo, Z.Y.; Yuan, J.; Li, M.F.; She, Z.G.; Lin, Y.C. The bioactive metabolites of the mangrove endophytic fungus *Talaromyces* sp. ZH-154 isolated from *Kandelia candel* (L.) Druce. *Planta Med.* **2010**, *76*, 185–189. [[CrossRef](#)] [[PubMed](#)]
10. Bara, R.; Aly, A.H.; Pretsch, A.; Wray, V.; Wang, B.; Proksch, P.; Debbab, A. Antibiotically active metabolites from *Talaromyces wortmannii*, an endophyte of *Aloe vera*. *J. Antibiot.* **2013**, *66*, 491–493. [[CrossRef](#)] [[PubMed](#)]
11. Zhai, M.M.; Li, J.; Jiang, C.X.; Shi, Y.P.; Di, D.L.; Crews, P.; Wu, Q.X. The bioactive secondary metabolites from *Talaromyces* species. *Nat. Prod. Bioprospect.* **2016**, *6*, 1–24. [[CrossRef](#)] [[PubMed](#)]
12. Yilmaz, N.; Visagie, C.M.; Houbraken, J.; Frisvad, J.C.; Samson, R.A. Polyphasic taxonomy of the genus *Talaromyces*. *Stud. Mycol.* **2014**, *78*, 175–341. [[CrossRef](#)] [[PubMed](#)]
13. Ghisalberti, E.L.; Hargreaves, J.R.; McConville, E. Butenolides from a cultured microfungus, *Acremonium* sp. *Nat. Prod. Res.* **2004**, *18*, 105–109. [[CrossRef](#)] [[PubMed](#)]
14. Ancheeva, E.; Küppers, L.; Akone, S.H.; Ebrahim, W.; Liu, Z.; Mándi, A.; Kurtán, T.; Lin, W.; Orfali, R.; Rehberg, N.; et al. Expanding the metabolic profile of the fungus *Chaetomium* sp. through co-culture with autoclaved *Pseudomonas aeruginosa*. *Eur. J. Org. Chem.* **2017**, *2017*, 3256–3264. [[CrossRef](#)]
15. Pescitelli, G.; Bruhn, T. Good computational practice in the assignment of absolute configurations by TDDFT calculations of ECD spectra. *Chirality* **2016**, *28*, 466–474. [[CrossRef](#)] [[PubMed](#)]
16. Mándi, A.; Mudianta, I.W.; Kurtán, T.; Garson, M.J. Absolute configuration and conformational study of psammaphysins A and B from the Balinese marine sponge *Aplysinella strongylata*. *J. Nat. Prod.* **2015**, *78*, 2051–2056. [[CrossRef](#)] [[PubMed](#)]
17. Barrow, C.J. New macrocyclic lactones from a *Penicillium* species. *J. Nat. Prod.* **1997**, *60*, 1023–1025. [[CrossRef](#)]
18. Xu, Y.; Zhou, T.; Espinosa-Artiles, P.; Tang, Y.; Zhan, J.; Molnár, I. Insights into the biosynthesis of 12-membered resorcylic acid lactones from heterologous production in *Saccharomyces cerevisiae*. *ACS Chem. Biol.* **2014**, *9*, 1119–1127. [[CrossRef](#)] [[PubMed](#)]
19. Zhang, P.; Meng, L.H.; Mándi, A.; Li, X.M.; Kurtán, T.; Wang, B.G. Structure, absolute configuration, and conformational study of resorcylic acid derivatives and related congeners from the fungus *Penicillium brocae*. *RSC Adv.* **2015**, *5*, 39870–39877. [[CrossRef](#)]
20. An, Y.N.; Zhang, X.; Zhang, T.Y.; Zhang, M.Y.; Zhang, Q.; Deng, X.Y.; Zhao, F.; Zhu, L.J.; Wang, G.; Zhang, J.; et al. Penicimenolides A–F, resorcylic acid lactones from *Penicillium* sp., isolated from the rhizosphere soil of *Panax notoginseng*. *Sci. Rep.* **2016**, *6*, 27396–27409. [[CrossRef](#)] [[PubMed](#)]
21. Kerti, G.; Kurtán, T.; Illyés, T.Z.; Kövér, K.E.; Sólyom, S.; Pescitelli, G.; Fujioka, N.; Berova, N.; Antus, S. Enantioselective synthesis of 3-methylisochromans and determination of their absolute configurations by circular dichroism. *Eur. J. Org. Chem.* **2007**, 296–305. [[CrossRef](#)]
22. Krohn, K.; Kock, I.; Elsässer, B.; Flörke, U.; Schulz, B.; Dräger, S.; Pescitelli, G.; Antus, S.; Kurtán, T. Bioactive natural products from the endophytic fungus *Ascochyta* sp. from *melilotus dentatus*—Configurational assignment by solid-state CD and TDDFT calculations. *Eur. J. Org. Chem.* **2007**, 1123–1129.
23. Hussain, H.; Akhtar, N.; Dräger, S.; Schulz, B.; Pescitelli, G.; Salvadori, P.; Antus, S.; Kurtán, T.; Krohn, K. New bioactive 2,3-epoxycyclohexenes and isocoumarins from the endophytic fungus *Phomopsis* sp. from *Laurus azorica*. *Eur. J. Org. Chem.* **2009**, 749–756. [[CrossRef](#)]
24. Li, S.; Wei, M.; Chen, G.; Lin, Y. Two new dihydroisocoumarins from the endophytic fungus *Aspergillus* sp. collected from the South China Sea. *Chem. Nat. Compd.* **2012**, *48*, 371–373. [[CrossRef](#)]
25. Yadav, J.S.; Mishra, A.K.; Dachavaram, S.S.; Kumar, S.G.; Das, S. First enantioselective total synthesis of penicimarin B, aspergillumarins A and B. *Tetrahedron Lett.* **2014**, *55*, 2921–2923. [[CrossRef](#)]
26. El Amrani, M.; Debbab, A.; Aly, A.H.; Wray, V.; Dobretsov, S.; Müller, W.E.G.; Lin, W.; Lai, D.; Proksch, P. Farinomalein derivatives from an unidentified endophytic fungus isolated from the mangrove plant *Avicennia marina*. *Tetrahedron Lett.* **2012**, *53*, 6721–6724. [[CrossRef](#)]
27. Ebrahim, W.; Aly, A.H.; Mándi, A.; Totzke, F.; Kubbutat, M.H.G.; Wray, V.; Lin, W.H.; Dai, H.; Proksch, P.; Kurtán, T.; et al. Decalactone derivatives from *Corynespora cassiicola*, an endophytic fungus of the mangrove plant *Laquncularia racemosa*. *Eur. J. Org. Chem.* **2012**, *2012*, 3476–3484. [[CrossRef](#)]
28. Zhuravleva, O.I.; Sobolevskaya, M.P.; Leshchenko, E.V.; Kirichuk, N.N.; Denisenko, V.A.; Dmitrenok, P.S.; Dyshlovoy, S.A.; Zakharenko, A.M.; Kim, N.Y.; Afiyatullo, S.S. Meroterpenoids from the alga-derived fungi *Penicillium thomii* Maire and *Penicillium lividum* Westling. *J. Nat. Prod.* **2014**, *77*, 1390–1395. [[CrossRef](#)] [[PubMed](#)]

29. Chen, J.; Chen, J.J.; Yang, L.Q.; Hua, L.; Gao, K. Labdanediterpenoids and shikimic acid derivatives from *Araucaria cunninghamii*. *Planta Med.* **2011**, *77*, 485–488. [[CrossRef](#)] [[PubMed](#)]
30. Dar, A.A.; Dangroo, N.A.; Raina, A.; Qayum, A.; Singh, S.; Kumar, A.; Sangwan, P.L. Biologically active xanthenes from *Codonopsis ovate*. *Phytochemistry* **2016**, *132*, 102–108. [[CrossRef](#)] [[PubMed](#)]
31. Kjer, J.; Debbab, A.; Aly, A.H.; Proksch, P. Methods for isolation of marine-derived endophytic fungi and their bioactive secondary products. *Nat. Protoc.* **2010**, *5*, 479–490. [[CrossRef](#)] [[PubMed](#)]
32. Grimme, S. Semiempirical GGA-type density functional constructed with a long-range dispersion correction. *J. Comput. Chem.* **2006**, *27*, 1787–1799. [[CrossRef](#)] [[PubMed](#)]
33. Sun, P.; Xu, D.X.; Mándi, A.; Kurtán, T.; Li, T.J.; Schulz, B.; Zhang, W. Structure, absolute configuration, and conformational study of 12-membered macrolides from the fungus *Dendrodochium* sp. associated with the sea cucumber *Holothuria nobilis* Selenka. *J. Org. Chem.* **2013**, *78*, 7030–7047. [[CrossRef](#)] [[PubMed](#)]
34. Yanai, T.; Tew, D.P.; Handy, N.C. A new hybrid exchange–correlation functional using the Coulomb-attenuating method (CAM-B3LYP). *Chem. Phys. Lett.* **2004**, *393*, 51–57. [[CrossRef](#)]
35. Frisch, M.J.; Trucks, G.W.; Schlegel, H.B.; Scuseria, G.E.; Robb, M.A.; Cheeseman, J.R.; Scalmani, G.; Barone, V.; Mennucci, B.; Petersson, G.A.; et al. *Gaussian 09*, revision B.01; Gaussian, Inc.: Wallingford, CT, USA, 2010.
36. Stephens, P.J.; Harada, N. ECD cotton effect approximated by the Gaussian curve and other methods. *Chirality* **2010**, *22*, 229–233. [[CrossRef](#)] [[PubMed](#)]
37. MacroModel. Schrödinger, LLC, 2015. Available online: <http://www.schrodinger.com/> (accessed on 31 December 2013).
38. Varetto, U. *MOLEKEL*, version 5.4; Swiss National Supercomputing Centre: Manno, Switzerland, 2009.
39. Ashour, M.; Edrada, R.; Ebel, R.; Wray, V.; Wätjen, W.; Padmakumar, K.; Müller, W.E.G.; Lin, W.H.; Proksch, P. Kahalalide derivatives from the Indian sacoglossan mollusk *Elysia grandifolia*. *J. Nat. Prod.* **2006**, *69*, 1547–1553. [[CrossRef](#)] [[PubMed](#)]
40. Clinical and Laboratory Standards Institute (CLSI). *Methods for Dilution Antimicrobial Susceptibility Tests for Bacteria That Grow Aerobically: Approved Standard*, 9th ed.; Clinical and Laboratory Standards Institute: Wayne, PA, USA, 2012.



© 2017 by the authors. Licensee MDPI, Basel, Switzerland. This article is an open access article distributed under the terms and conditions of the Creative Commons Attribution (CC BY) license (<http://creativecommons.org/licenses/by/4.0/>).